Lawrence Berkeley Laboratory
UNIVERSITY OF CALIFORNIA

Physics, Computer Science & Mathematics Division

To be presented at the 7th Society of Petroleum Engineers Reservoir Simulation Symposium, San Francisco, CA, November 15-18, 1983

NUMERICAL SOLUTION OF THE BUCKLEY-LEVERETT EQUATIONS

J. Sethian, A.J. Chorin, and P. Concus

September 1983

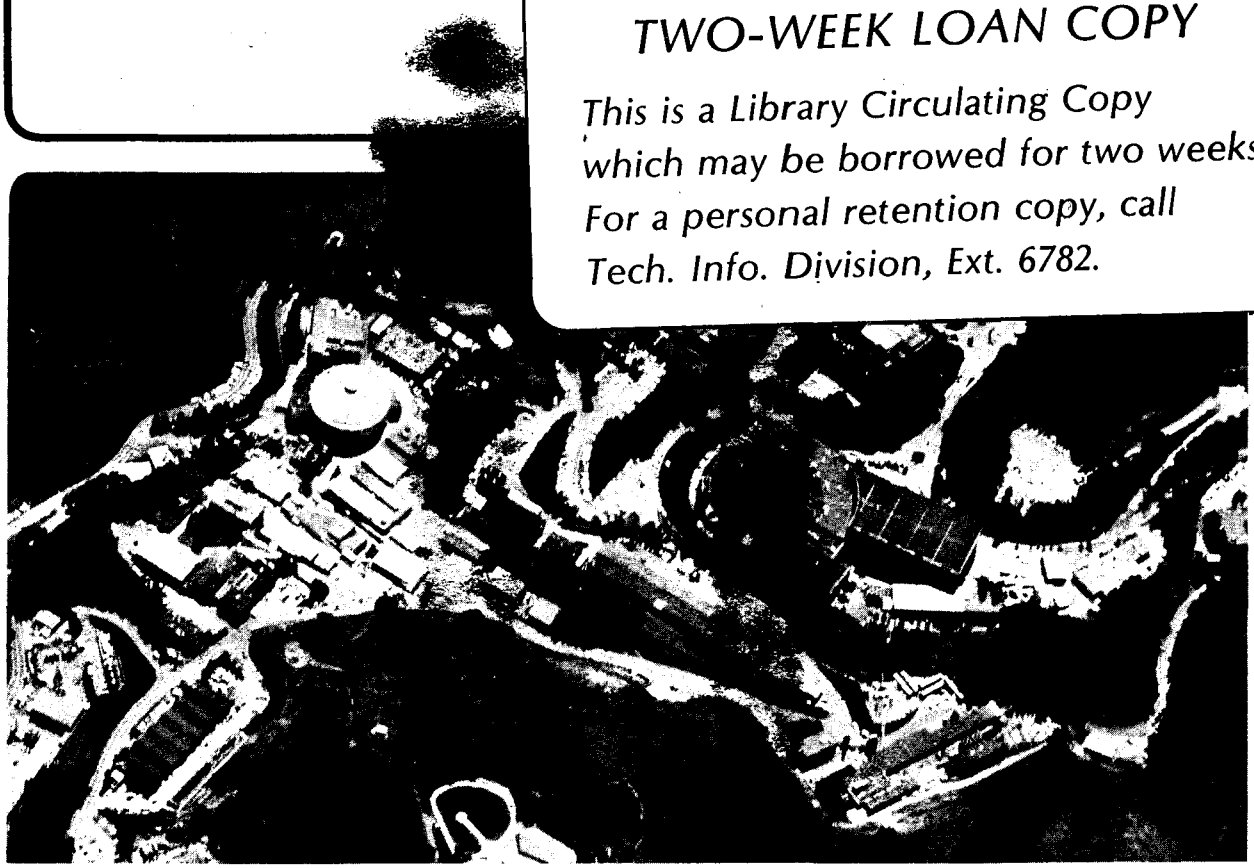

Prepared for the U.S. Department of Energy under Contract DE-AC03-76SF00098

DISCLAIMER

LBL-16587

Numerical Solution of the Buckley-Leverett Equations

James Sethian, Alexandre Joel Chorin, and Paul Concus

Department of Mathematics
and
Lawrence Berkeley Laboratory
University of California
Berkeley, California, 94720

This work was supported in part by the International Business Machines Corporation, Palo Alto Scientific Center, Palo Alto, CA, and by the Director, Office of Basic Energy Sciences, Engineering, Mathematical, and Geosciences Division of the U.S. Department of Energy under Contract DE-AC03-76SF00098.

ABSTRACT

A modified random choice method is described for solving simultaneously the Buckley-Leverett, incompressibility, and Darcy's Law equations for immiscible displacement in a porous medium. The main idea of the numerical method is to modify the one-dimensional Riemann solvers in the split random choice method so that the multidimensional flow is represented correctly. Other features include flux conserving differencing of pressure and velocity and an accurate description of sources and sinks. Numerical results for a two-dimensional five-spot waterflood indicate that the advancing front is kept sharp by the method, that the time of breakthrough is accurate, and that grid orientation effects are unimportant.

INTRODUCTION

A central problem in petroleum reservoir simulation is to model the displacement of one fluid by another within a porous medium. Such problems may be characterized by the injection of a wetting fluid, (e.g. water), into the reservoir at one point, displacing the non-wetting fluid (e.g. oil), which is being withdrawn at another point. The nature of the front between the non-wetting fluid and the wetting fluid is of primary importance; one would like to withdraw as much oil as possible before water reaches the recovery point. A particularly troublesome phenomenon associated with the above procedure is fingering, in which small channels of water push through the oil towards the recovery point, leaving oil behind.

In the design of numerical techniques to model petroleum reservoir recovery, one is faced with the problem that the solution to the fluid saturation equations describing the saturation within the reservoir at any time can develop sharp fronts or discontinuities. Finite difference approximations to these equations smear out the front and may distort the nature of the interface, unless expensive mesh refinement is used. One can instead attempt to track the front between the two fluids; however, such techniques usually contain an intrinsic smoothing and thus can predict a stable interface in regimes where fingering should occur. An alternative to the above techniques, which serves as a foundation for the work presented here, is the random choice method, in which the generation of the solution at each time step is based on the exact solution of a collection of local Riemann problems.

In this paper, we apply a recently developed generalized version of the one-dimensional random choice method to a problem in two-dimensional reservoir simulation. In this improved technique, while the multi-dimensional solution is obtained through a sequence of one-dimensional problems, information about the two-dimensional solution is used to ensure that each of the one-dimensional problems correctly interprets the nature of the discontinuity. Another aspect of our algorithm is the formulation of flux conserving difference equations for the pressure and velocity, thus ensuring the conservation of fluid volume in each cell. The above algorithm was first used in [3] to study the nature of fingering instability. A third aspect of our algorithm is the representation of sources and sinks in the pressure calculation in a natural way through a flux form of the boundary conditions for the velocity.

We apply our technique to a two-dimensional five spot waterflood problem. Experiments were performed over a variety of grid sizes and orientations. Our results indicate that the advancing front is kept sharp, that the time of breakthrough is accurate, and that grid orientation effects are unimportant.

EQUATIONS OF MOTION

We consider the equations

$$\frac{\partial s}{\partial t} + \vec{u}\cdot\nabla[f(s)] = 0 \tag{1}$$

$$\nabla\cdot\vec{u} = 0 \tag{2}$$

References and figures are at the end of the paper.

$$\vec{u} = -\lambda(s)\nabla p \ , \tag{3}$$

where $s = s(x,y,t)$ is the saturation (the fraction of available volume at the point (x,y) and time t filled with wetting fluid, e.g. water), $\vec{u} = \vec{u}(x,y,t)$ is the total velocity of the fluid, $p = p(x,y,t)$ is the pressure, $\lambda(s)$ is the total mobility and $f(s)$ is the fractional flow function. Equations (1), (2), and (3), known as the Buckley-Leverett equation, incompressibility relation, and Darcy's Law, respectively, describe the flow of two immiscible, incompressible fluids through a homogeneous porous medium in the absence of capillary pressure and gravitational effects, see [8,9]. For immiscible fluids, we take the total mobility $\lambda(s)$ to be represented by

$$\lambda(s) = s^2 + (1-s)^2/\mu \ , \tag{4}$$

where μ is the ratio of the viscosity of the non-wetting fluid to that of the wetting fluid. The corresponding fractional flow function $f(s)$ is

$$f(s) = s^2/\lambda(s) \ . \tag{5}$$

Equations (2) and (3) together form an elliptic equation. Equation (1) is hyperbolic and as such can develop discontinuities in s, even for arbitrarily smooth initial data. To analyze the nature of these discontinuities, we consider (1) in one space dimension, namely,

$$s_t + (f(s))_x = s_t + f'(s)s_x = 0 \ . \tag{6}$$

Here, we have taken the velocity as unity to simplify the discussion.

Suppose for a given problem the fractional flow function satisfies $f_{ss} > 0$ and thus f is concave up. It can easily be shown that the characteristics for (6) are straight lines leaving the x-axis with slope

$$\frac{dx}{dt} = f'(s) \ . \tag{7}$$

Since $f_{ss} > 0$, then $f'(s)$ is an increasing function of s. Consider the initial data

$$s(x,0) = \begin{cases} s_l \ , & x < 0 \\ s_r \ , & x > 0 \end{cases} , \tag{8}$$

where s_l and s_r are constants. If $s_l < s_r$, then $f'(s_l) < f'(s_r)$ and information from the left is propagating slower than information from the right. The entropy condition, which requires that all characteristics reach back to the initial data, thus dictates that a rarefaction wave will form between the two (see Fig. 1). Conversely, if $s_l > s_r$, then $f'(s_l) > f'(s_r)$, and information from the left propagates faster than information from the right; the entropy condition thus dictates the formation of a shock propagating with speed $\dfrac{f(s_r) - f(s_l)}{s_r - s_l}$ (Fig. 2).

In the case of more general f, one has the generalized entropy condition (Oleinik's condition E), which determines the type of admissible shocks: Given s_- and s_+, where s_- and s_+ are the limiting values to the left and the right of a discontinuity, respectively, a solution to (6) exists, is unique, and depends continuously on the initial data if the following holds

1) if $s_- < s_+$ then $\dfrac{f(s_+) - f(s_-)}{s_+ - s_-} \leq \dfrac{f(s_+) - f(s)}{s_+ - s}$

for all $s \in [s_-, s_+]$.

2) if $s_+ < s_-$ then $\dfrac{f(s_+) - f(s_-)}{s_+ - s_-} \geq \dfrac{f(s_+) - f(s)}{s_+ - s}$

for all $s \in [s_+, s_-]$.

Geometrically, this condition translates into the statement that admissible shocks are those such that (1) if $s_- < s_+$, then the chord connecting $(s_-, f(s_-))$ and $(s_+, f(s_+))$ must lie below f, (2) if

$s_+ < s_-$, then the chord connecting $(s_+, f(s_+))$ and $(s_-, f(s_-))$ must lie above f. In the case of a purely convex f, the above produces the situations described earlier; in particular, a shock cannot be allowed to connect the left state with the right state in Fig. 1. For non-convex f, the above condition also rules out such waves as shocks which move faster or slower than the characteristics on both of their sides.

In our problem, the fractional flow function (5) contains one inflection point (see Fig. 3). Thus the wave connecting the left and right states will be either a shock, rarefaction, or combination of the two. We determine the appropriate wave as follows. Given s_l and s_r, the left and right states respectively,

1) If the chord connecting $(s_l, f(s_l))$ and $(s_r, f(s_r))$ does not intersect f, then the curve is convex up or down between the two points. If $f'(s_l) > f'(s_r)$, then by the generalized entropy condition a shock must connect s_l with s_r; if $f'(s_l) < f'(s_r)$, then a rarefaction connects the two states.

2) Suppose the chord connecting the left and right states intersects f. Then there exists a point s_* between s_r and s_l such that the chord from $(s_r, f(s_r))$ to $(s_*, f(s_*))$ is tangent to f at $(s_*, f(s_*))$ (the case $s_r < s_l$ is shown in Fig. 4.). The wave connecting s_r to s_* is a shock and the wave connecting s_* to s_l is a rarefaction.

The above choices apply to the case in which the advection velocity u is equal to one. If u is positive, the wave speeds are merely scaled by u. If u is negative, the roles of s_l and s_r are interchanged in the above arguments.

NUMERICAL ALGORITHM

For the purposes of this discussion we consider the standard diagonal geometry quarter five spot problem. That is, we assume a square domain D, centered at $(\frac{1}{2},\frac{1}{2})$, with sides of unit length, and (1)-(3) holding inside the domain. At (0,0) we place a source of unit strength; at (1,1) we place a sink of unit strength. We have the initial conditions

$$s(x,y,0) = 0 \quad \text{for} \quad (x,y) \neq (0,0)\,, \tag{9}$$

together with the boundary conditions

$$s(0,0,t) = 1 \tag{10}$$

$$\frac{\partial s}{\partial \vec{n}} = \frac{\partial p}{\partial \vec{n}} \text{ on the edges of the square}\,, \tag{11}$$

where $\vec{n}$ is the normal to the boundary. The above problem may be summarized by saying that we inject wetting fluid ($s = 1$, water) into the lower left corner with strength so that the flux is equal to unity, and withdraw non-wetting fluid ($s = 0$, oil) from the upper right corner at the same rate; at no other points can fluid enter or leave the domain.

The numerical algorithm used to solve the equations of motion is based on a generalized random choice method for the hyperbolic equation (1) coupled to a successive over-relaxation method for the elliptic equation (2),(3). The random choice method is a numerical technique developed in [2] and is based on a constructive existence proof introduced in [7]. We briefly describe the technique below.

Consider the equation

$$s_t + u[f(s)]_x = 0\,. \tag{12}$$

Place a uniformly spaced grid of mesh length h along the x axis and let s_i^n be the value $s(ih, n\Delta t)$; thus we view s as a piecewise constant function, constant within each interval $[(i-\frac{1}{2})h, (i+\frac{1}{2})h]$. This produces a collection of initial value Riemann problems of the form

$$s = \begin{cases} s_l \ , & x < (i+\tfrac{1}{2})h \\ s_r \ , & x > (i+\tfrac{1}{2})h \end{cases}, \tag{13}$$

where $s_l = s_i^n$ and $s_r = s_{i+1}^n$. The solution is then updated in time by solving each Riemann problem exactly, with the type of wave used to connect the two states (shock, rarefaction, compound) determined by means of the arguments presented earlier. The solution is then sampled to produce new values of s; we use a sampling based on a van der Corput sequence, see [4]. The time step Δt is chosen to be the largest possible value such that the separate Riemann problems do not intersect; that is,

$$\Delta t \, |u| \max_i f'(s_i^n) \leq h \ . \tag{14}$$

This technique was first applied to porous flow problems in [5].

A natural way to extend the above one-dimensional technique to two dimensions is to split the two-dimensional hyperbolic equation

$$s_t + \vec{u} \cdot \nabla [f(s)] = 0 \tag{15}$$

into two steps; first a one-dimensional problem in the x direction

$$s_t + u \frac{\partial}{\partial x}(f(s)) = 0 \tag{16}$$

is solved, followed by a one-dimensional problem in the y direction

$$s_t + v \frac{\partial}{\partial y}(f(s)) = 0 \ , \tag{17}$$

where the velocity $\vec{u} = (u,v)$. Unfortunately, a front not parallel to either the x or y axis can be misinterpreted during one of the sweeps, as may be seen by considering the following example. Suppose the interface between water and oil is lying diagonal to the grid, and the velocity vector at a point on the front is as shown in Fig. 5. It is clear that water is displacing oil, however if one looks simply at the component of the velocity vector in the x direction, oil seems to be displacing water and hence the solution to the one-dimensional problem will not accurately portray what is happening. Errors due to the above phenomenon can be significant; examples of their effect may be found in [6]. The technique we use, introduced in [3], first determines the correct orientation by analyzing the two-dimensional situation, and uses this information in each of the one-dimensional sweeps.

We now describe the algorithm for solving Equations (1)-(3). With time step Δt, let $s_{i,j}^n$ be the value of the saturation at $s(ih, jh, n\Delta t)$; here we assume that $s_{i,j}^n$ is defined on a square grid i,j of mesh length h imposed on the domain. The pressures $p_{i,j}^n$ are taken at the same grid points, and the velocities $u_{i+\frac{1}{2},j}$, $v_{i,j+\frac{1}{2}}$ are to be evaluated at the midpoints of the sides of a cell (see Fig. 6). Assuming $s_{i,j}^n$ is known, we now describe the algorithm used to obtain $s_{i,j}^{n+1}$ from $s_{i,j}^n$.

The first step is to calculate $p_{i,j}^n$. Equation (2) may be substituted into (3) to obtain an expression involving only p and $\lambda(s)$, namely

$$\nabla \cdot (-\lambda(s) \nabla p) = 0 \tag{18}$$

It is natural to view (18) as a statement about the divergence of each cell i,j, hence a reasonable finite difference approximation to the left-hand side of (18), based on our staggered grid, is

$$\frac{(-\lambda(s)\nabla p)_{i+\frac{1}{2},j} - (-\lambda(s)\nabla p)_{i-\frac{1}{2},j}}{h} + \frac{(-\lambda(s)\nabla p)_{i,j+\frac{1}{2}} - (-\lambda(s)\nabla p)_{i,j-\frac{1}{2}}}{h} \ . \tag{19}$$

To approximate the first term of (19), for example, we use (see Fig. 6)

$$(\lambda(s)\nabla p)_{i+\frac{1}{2},j} \approx \frac{(\lambda(s_{i+1,j}) + \lambda(s_{i,j}))\,(p_{i+1,j} - p_{i,j})}{2h} \ . \tag{20}$$

The full finite difference approximation to (18) at an interior point is thus given by

$$
\begin{aligned}
&- \frac{(\lambda(s_{i+1,j})+\lambda(s_{i,j}))(p_{i+1,j}-p_{i,j})}{2h^2} \\
&+ \frac{(\lambda(s_{i,j})+\lambda(s_{i-1,j}))(p_{i,j}-p_{i-1,j})}{2h^2} \\
&- \frac{(\lambda(s_{i,j+1})+\lambda(s_{i,j}))(p_{i,j+1}-p_{i,j})}{2h^2} \\
&+ \frac{(\lambda(s_{i,j})+\lambda(s_{i,j-1}))(p_{i,j}-p_{i,j-1})}{2h^2} = 0 .
\end{aligned}
\tag{21}
$$

The above scheme conserves the flux $-\lambda(s)\nabla p$ through each cell, and consequently ensures that there are no fictitious sources or sinks introduced by the finite difference approximation into our calculation.

Along the four sides, the discrete form of the boundary conditions (11) is used to modify (21). A technique sometimes employed to approximate the singularity at (0,0) is to extend (21) to include the injection cell and modify the right-hand side there to approximate a delta function with flux equal to unity. This might be done by setting the right-hand side equal to $1/h^2$, since the volume of the cell is h^2. Such a technique would yield an error in the computation of the pressure in the cells around (0,0).

To overcome this problem, rather than attempting to create a suitable compensating right-hand side, we choose to work directly with the requirement that the flux is unity through the injection cell. This is the same as taking the velocity normal to each side of the injection cell pointing outwards as equal to 1/4. Our technique is to require that $-\lambda(s)\nabla p$ be equal to this velocity at the edges of the injection cell. Analogous relations are formulated at the sink. Using these relations, we can close the system of algebraic equations (21) and solve for the pressure after evaluating $\lambda(s)$ using (4). There are a variety of ways to solve such systems; we have used an overrelaxation method with a position dependent relaxation factor. Once the pressures are obtained, we use our approximation to $\lambda(s)\nabla p$ to produce the velocities u and v.

With u^n , v^n, p^n and s^n known, we now solve (1) to determine s^{n+1} at the grid points. We first determine whether the two-dimensional advection velocity $\vec{u} = (u,v)$ causes water to displace oil or oil to displace water; this can easily be accomplished by checking the angle between $\vec{u}$ and ∇f. Then, we determine if the two one-dimensional sweeps

$$s_t + u\frac{\partial}{\partial x}(f(s)) = 0 \tag{22}$$

$$s_t + v\frac{\partial}{\partial y}(f(s)) = 0 \tag{23}$$

both interpret the situation in the same way as does the two-dimensional analysis. For example, if water is displacing oil, we check to see that the situation holds for both of the one-dimensional sweeps. If so, we may simply solve (22) and then (23) using the random choice method described earlier to obtain the new value s^{n+1}. Suppose, however, that one of the sweeps indicates an orientation different from the actual one described by the two-dimensional analysis; such a case is depicted in Fig. 5, in which, although water is clearly displacing oil, the x sweep indicates oil displacing water. In order to force the wave connecting the two states to be of the same type as that determined by the two-dimensional analysis, we switch the role of convex and concave hulls in our Riemann solution (this can be accomplished by interchanging s_l and s_r in the Riemann solver). Although the one-dimensional solution constructed may violate the generalized entropy condition (e.g. we now allow rarefaction shocks), the proper two-dimensional information is represented in each of the one-dimensional problems, and the generation of shocks and rarefaction waves due purely to grid orientation has been avoided. For details of the above algorithm, see [3].

RESULTS

In the first experiment, we modeled the test case of a source at (0,0), a sink at (1,1) and $\lambda(s) \mp 1$. In this situation, the elliptic equation uncouples from the hyperbolic equation, the pressure and velocity are independent of time, and an analytically derived solution can be found, see [1]. Such an example is useful as a first test to see how well a numerical technique determines the time until breakthrough, i.e., the time required for the wetting fluid to travel from the source to the sink. In [1], with injection at $t=0.0$, a breakthrough time of $t=2.132$ was determined from the analytically derived solution. We performed the simulation using a 20x20 and a 40x40 grid. In both cases, breakthrough was calculated at about $t=2.1$; this is in good agreement with the predicted value.

In the next set of experiments, on a 20x20 grid we computed the solution to the standard diagonal geometry quarter five-spot problem with $\lambda(s)$ given by (4) for $\mu=2$. In Fig. 7, the value of the saturation s is plotted as a surface above the x-y plane. The shock separating $s=0$ in the foreground (oil) from the water in the background is evident and clearly remains sharp. The results show the progression of the front from just after injection (Fig. 7a), to the circular shape in (Fig. 7b), to a square shape (Fig. 7c), to breakthrough (Fig. 7d). For comparison, the same problem was modeled on a 40x40 grid (Figs. 8a, 8b, 8c, and 8d).

In the final experiments, the effect of the orientation of the grid relative to the flow was examined. A standard way to do this (parallel geometry) is to consider a uniform grid on a square domain with sides of length $\sqrt{2}$, sources at (0,0) and $(\sqrt{2},\sqrt{2})$, and sinks at $(\sqrt{2},0)$ and $(0,\sqrt{2})$. This configuration corresponds to rotating the grid in the previous examples by 45 degrees. In Figs. 9a, 9b, 9c, and 9d, we show the results of such a calculation with a 56x56 grid spread over a $\sqrt{2} \times \sqrt{2}$ square; this provided approximately the same mesh length as in Fig. 8. As before, the front progresses from injection (Fig. 9a), through the circular shape of (Fig. 9b), through a square shape (Fig. 9c), to breakthrough (Fig. 9d). To make the comparison clearer, we provide contour plots of the saturation for the standard quarter five-spot problem on a 40×40 grid (Fig. 10a) and for the 56×56 rotated case, which has been interpolated onto the same 40×40 grid (Fig. 10b). Contour values of $s = .2, .3, \ldots, .9$ are plotted. Because of the interpolation required to rotate from the 56×56 grid to the 40×40 grid, and because the contour plotter displaces contours that should lie on top of each other, the shock at the front, clearly visible in the earlier figures, is now displayed as a dark band, and some oscillation in the front is produced. The shapes of the front are qualitatively the same, however, indicating that grid orientation effects are unimportant.

We remark that the numerical techniques discussed in this paper can easily be extended to three space dimensions.

ACKNOWLEDGMENTS

We are pleased to acknowledge Eric Kostlan for his participation in programming and carrying out the numerical examples. This work was supported in part by the International Business Machines Corporation, Palo Alto Scientific Center, Palo Alto, CA, and by the Director, Office of Basic Energy Sciences, Engineering, Mathematical, and Geosciences Division of the U.S. Department of Energy under Contract DE-AC03-76SF00098.

REFERENCES

1. Albright, N., Concus, P., and Proskurowski, W.: "Numerical Solution of the Multi-Dimensional Buckley-Leverett Equation by a Sampling Method", Paper SPE 7681, *Soc. Petrol. Eng. Fifth Symp. on Reservoir Simulation*, Denver, CO., Feb., 1979.

2. Chorin, A.J.: "Random Choice Solution of Hyperbolic Systems", *J. Comput. Phys.*, 22 (1976) 517-533.

3. Chorin, A.J.: "The Instability of Fronts in a Porous Medium", Lawrence Berkeley Laboratory Report LBL-15893, April 1983, to appear in *Comm. Math. Phys.*

4. Colella, P.: "Glimm's Method for Gas Dynamics", *SIAM J. Sci. Statist. Comput.*, 3 (1982) 76-110.

5. Concus, P. and Proskurowski, W.: "Numerical Solution of a Nonlinear Hyperbolic Equation by the Random Choice Method", *J. Comput. Phys.*, 30 (1979) 153-166.

6. Crandall, M. and Majda, A.: "The Method of Fractional Steps for Conservation Laws", *Numer. Math.*, 34 (1980) 285-314.

7. Glimm, J.: "Solution in the Large for Nonlinear Hyperbolic Systems of Equations", *Comm. Pure Appl. Math.*, 18 (1965) 697-715.

8. Peaceman, D.W.: *Fundamentals of Numerical Reservoir Simulation,* Elsevier, Amsterdam-Oxford-New York (1977).

9. Scheidegger, A.E.: *The Physics of Flow in Porous Media,* University of Toronto Press, Toronto (1974).

Figure Captions

Fig. 1. Riemann Problem Solution, Convex $f(s)$, $s_l < s_r$

Fig. 2. Riemann Problem Solution, Convex $f(s)$, $s_l > s_r$

Fig. 3. Fractional Flow Function

Fig. 4. Convex Hull for Compound Wave Solution, $s_l > s_r$

Fig. 5. Obliquely Propagating Discontinuity Front

Fig. 6. Staggered Grid for p, s, and $\vec{u}$

Fig. 7. Saturation for 20×20 Diagonal Grid
(a) $t = 0.39$ (b) $t = 1.20$
(c) $t = 1.99$ (d) $t = 2.11$

Fig. 8. Saturation for 40×40 Diagonal Grid
(a) $t = 0.39$ (b) $t = 1.19$
(c) $t = 2.00$ (d) $t = 2.15$

Fig. 9. Saturation for 56×56 Parallel Grid
(a) $t = 0.39$ (b) $t = 1.20$
(c) $t = 2.00$ (d) $t = 2.24$

Fig. 10. Saturation Contours $s = .2(.1).9$ at $t = 2.13$
(a) 40×40 Diagonal Grid
(b) 56×56 Parallel Grid

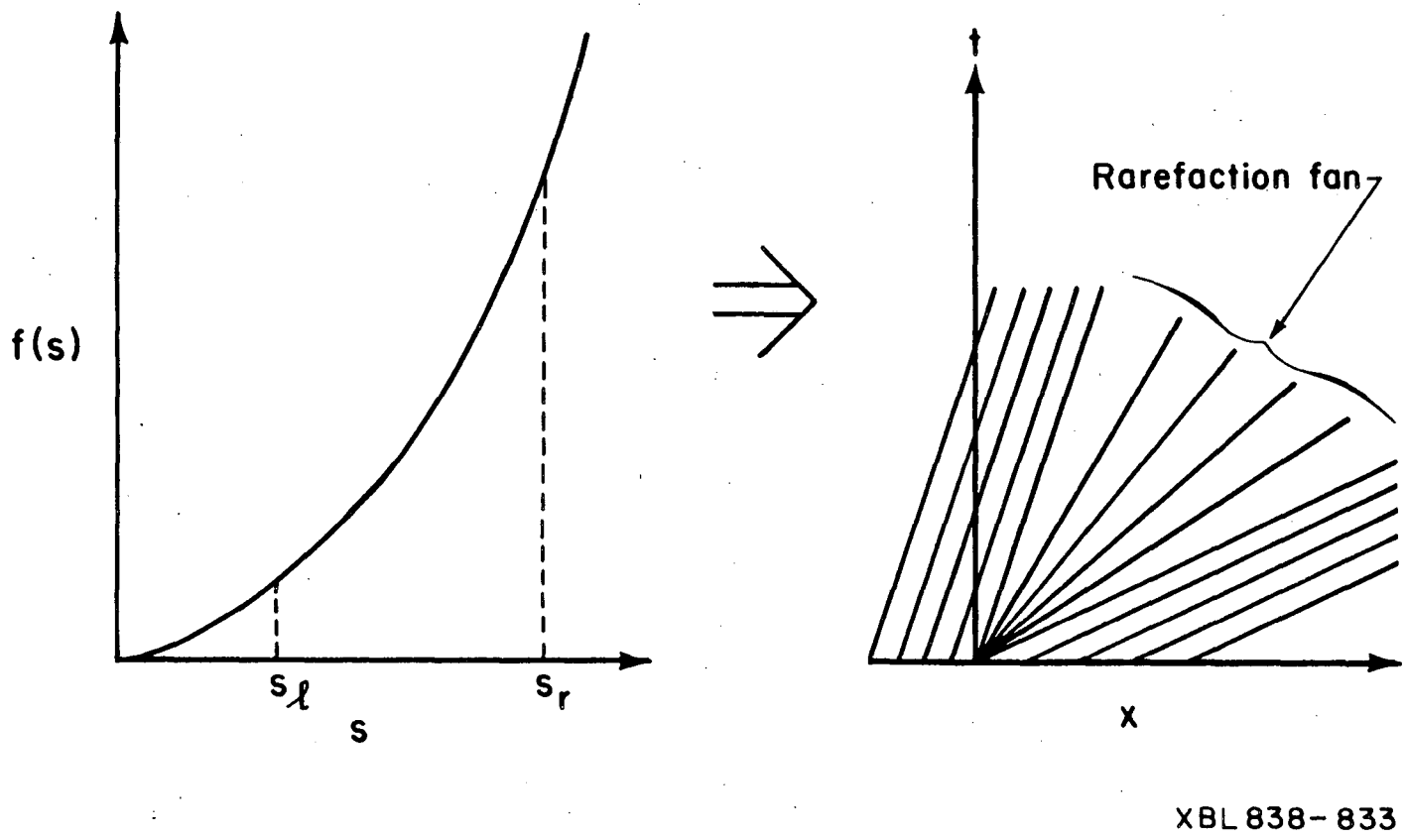

Fig. 1

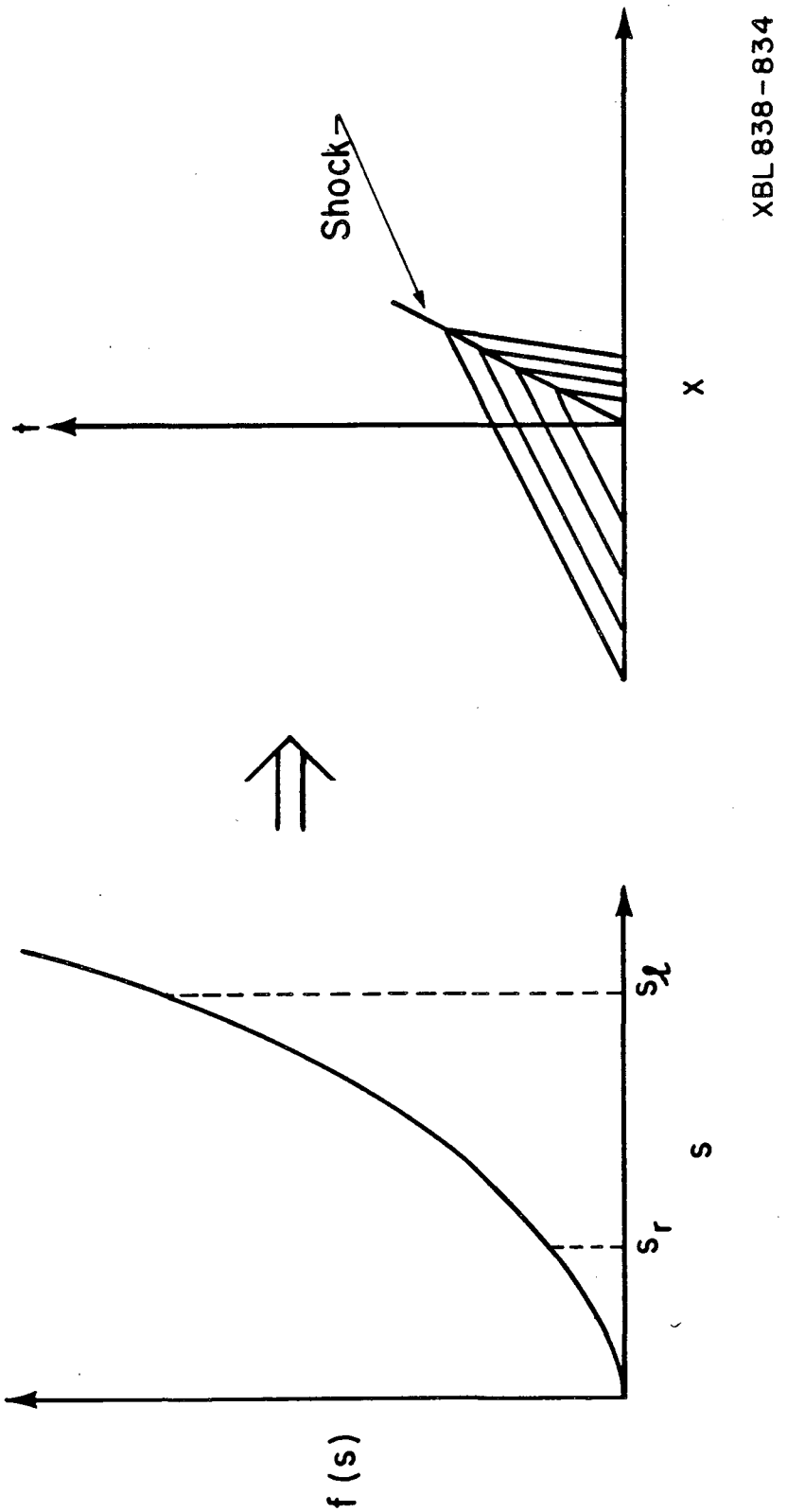

Fig. 2

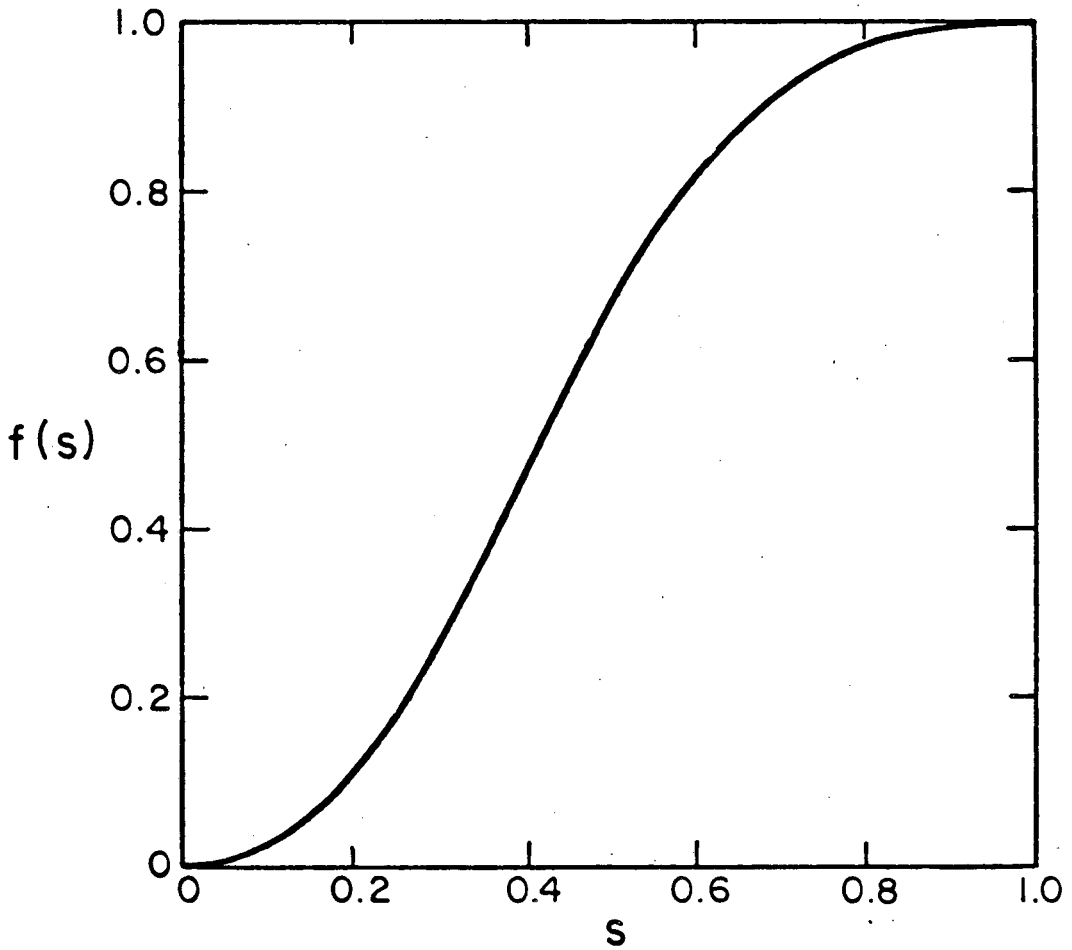

XBL838-830

Fig. 3

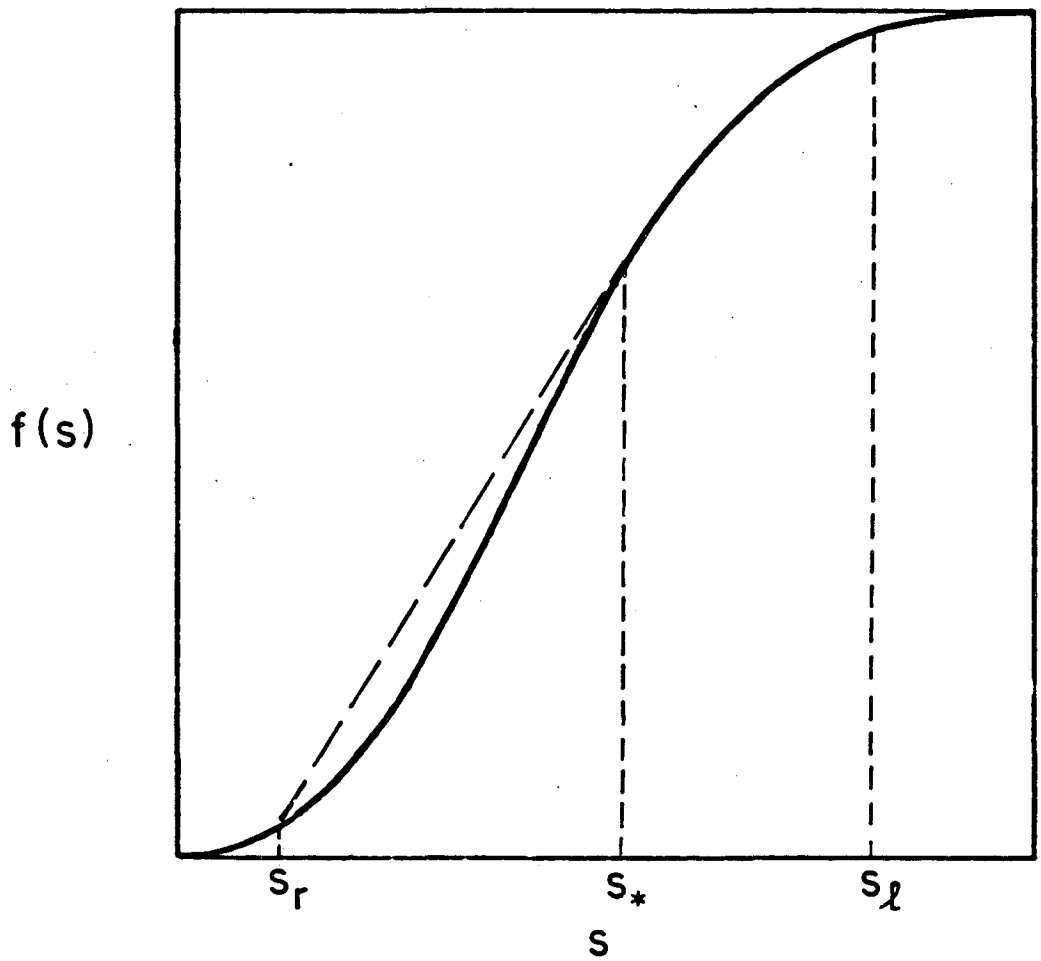

Fig. 4

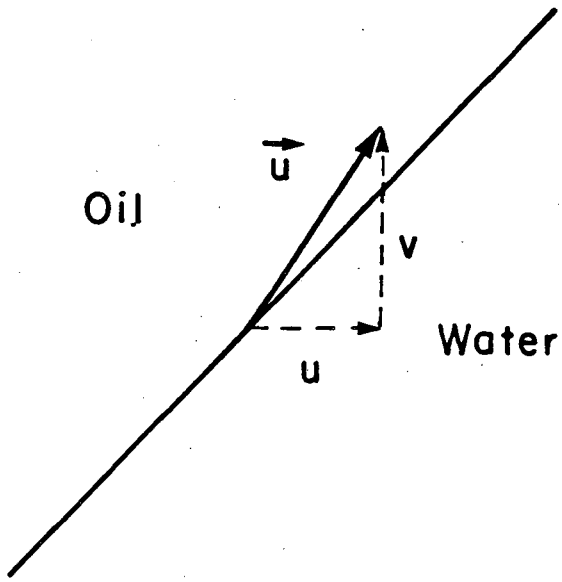

XBL838-835

Fig. 5

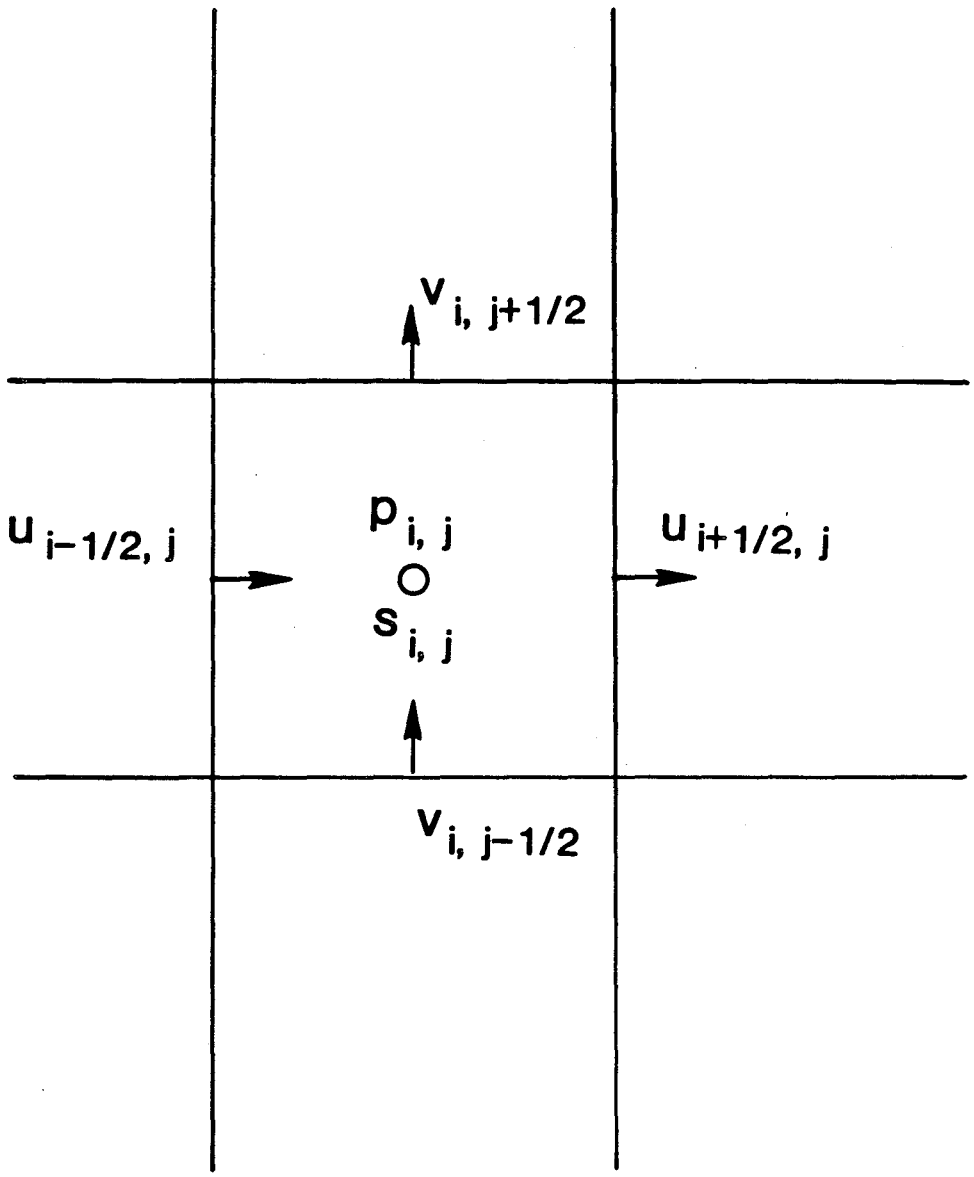

XBL 838-11207

Fig. 6

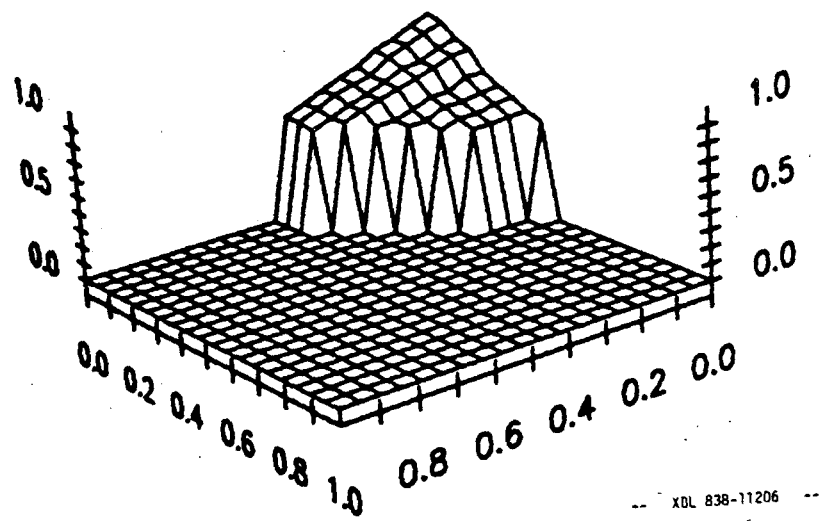

Fig. 7(a)

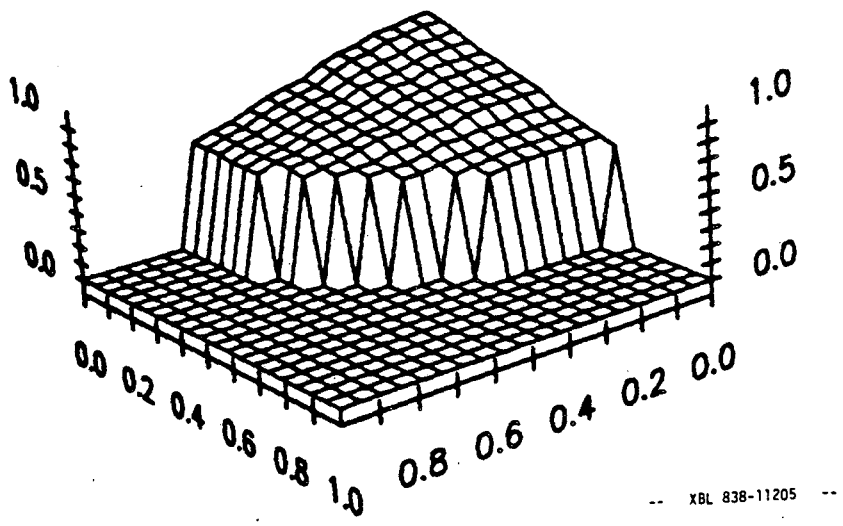

Fig. 7(b)

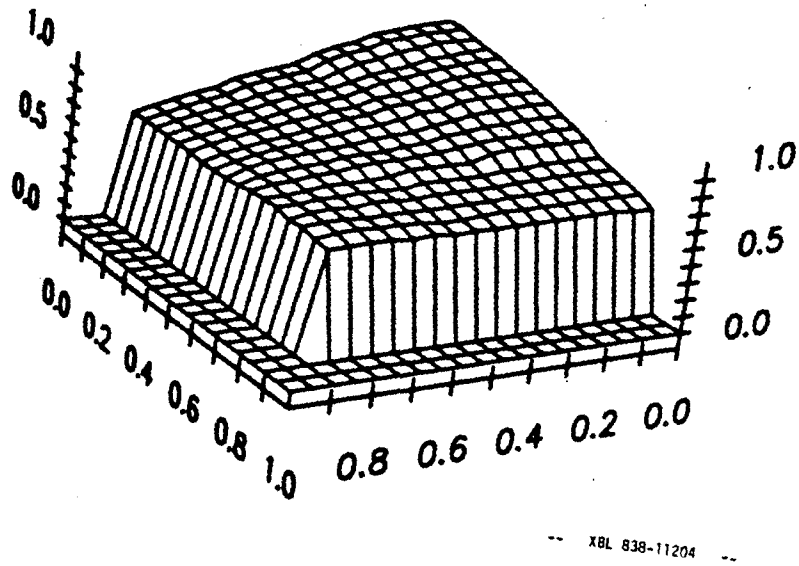

Fig. 7(c)

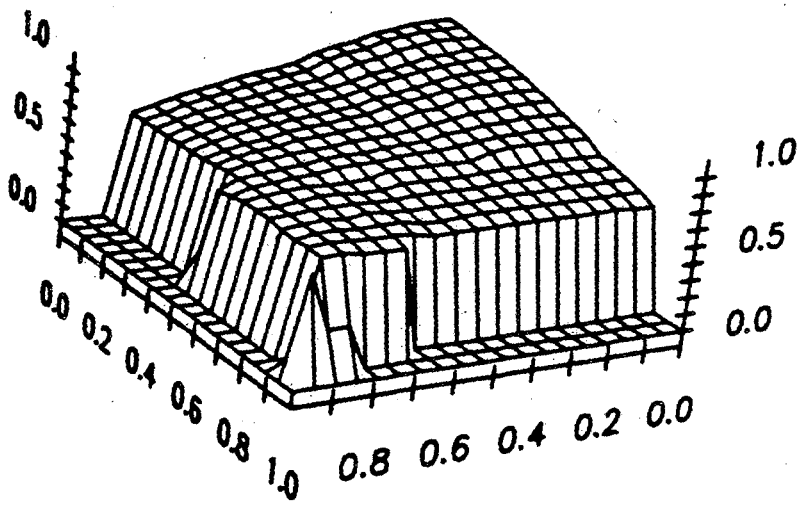

XBL 838-11203

Fig. 7(d)

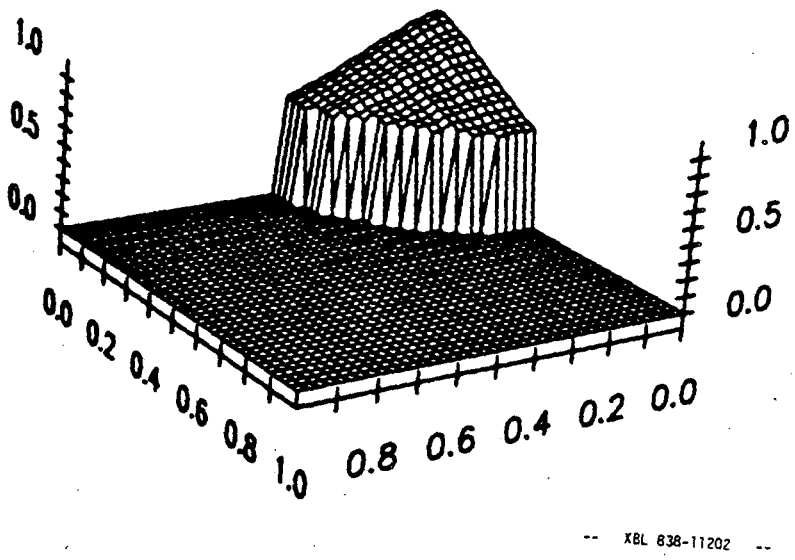

Fig. 8(a)

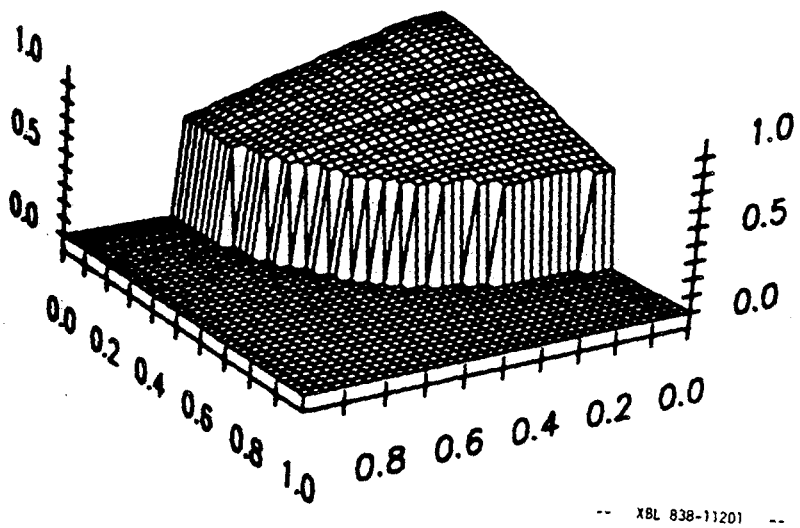

Fig. 8(b)

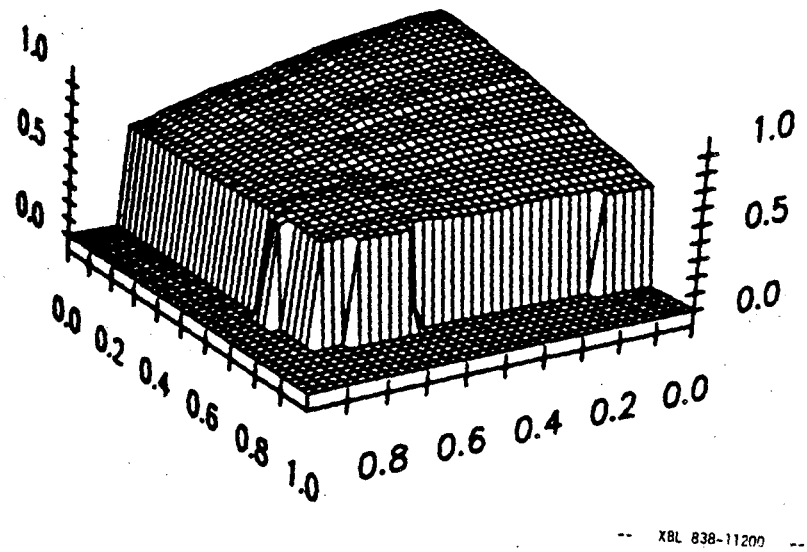

Fig. 8(c)

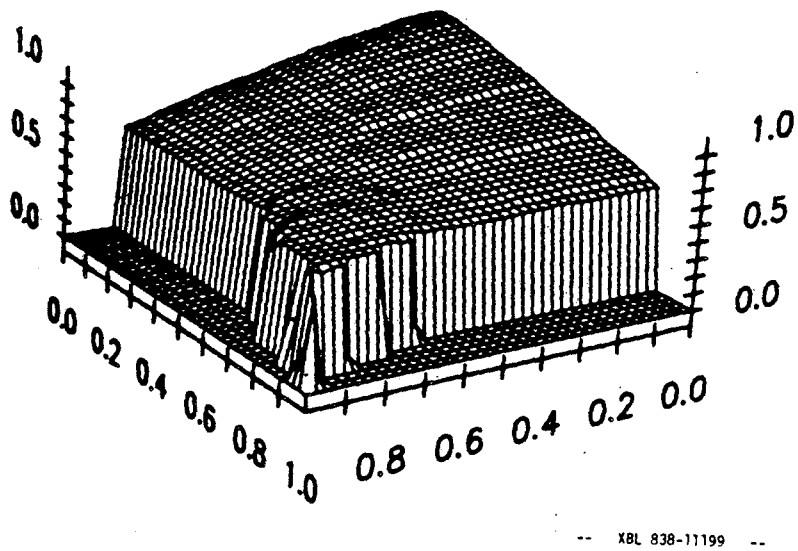

Fig. 8(d)

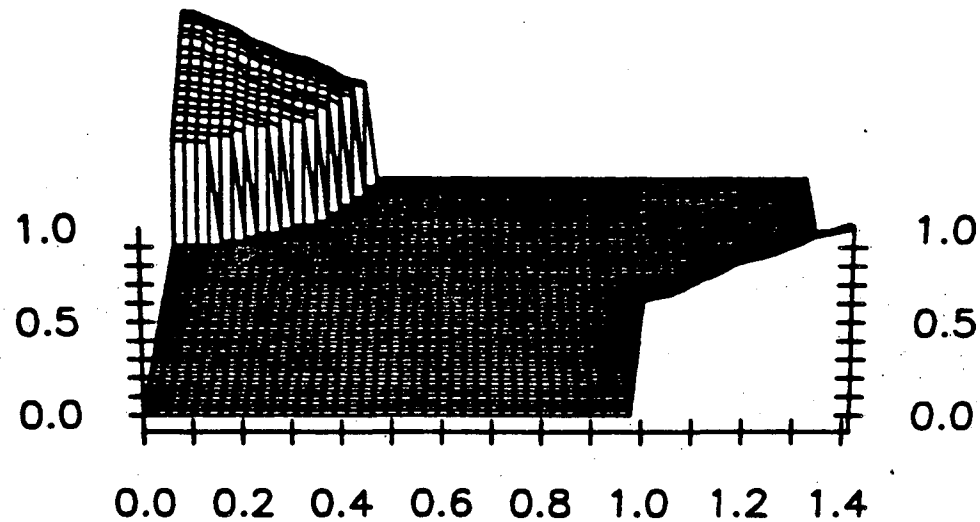

Fig. 9(a)

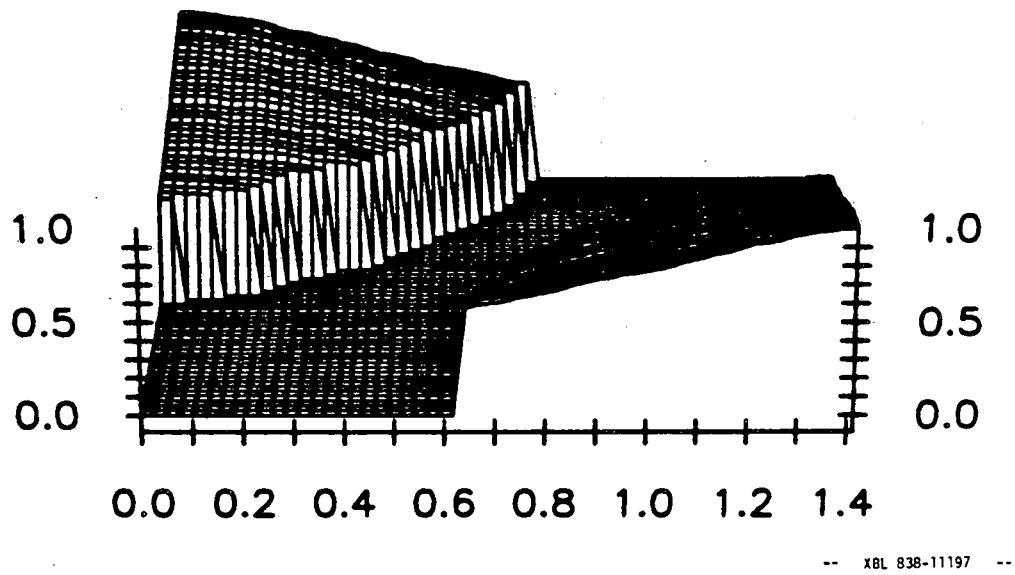

Fig. 9(b)

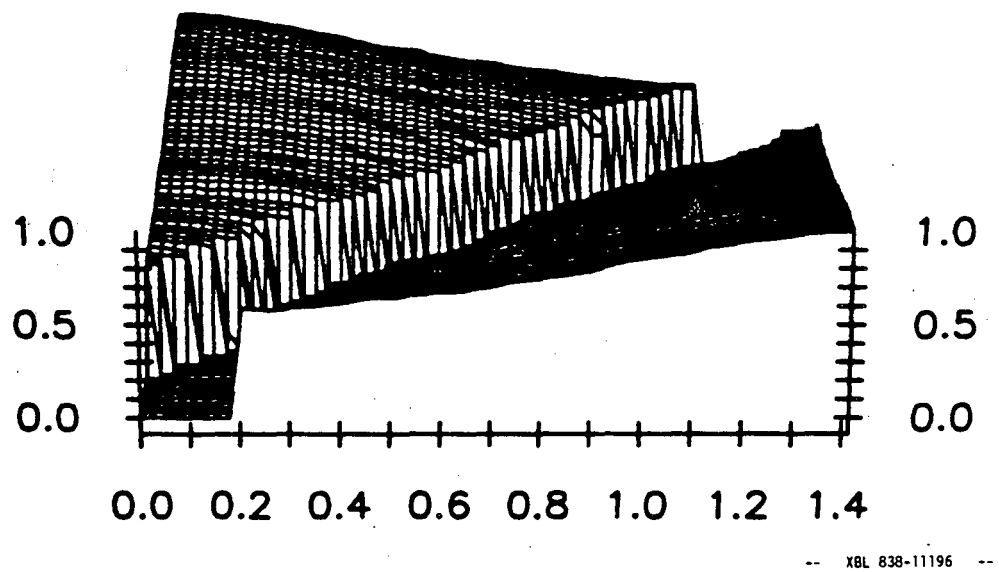

Fig. 9(c)

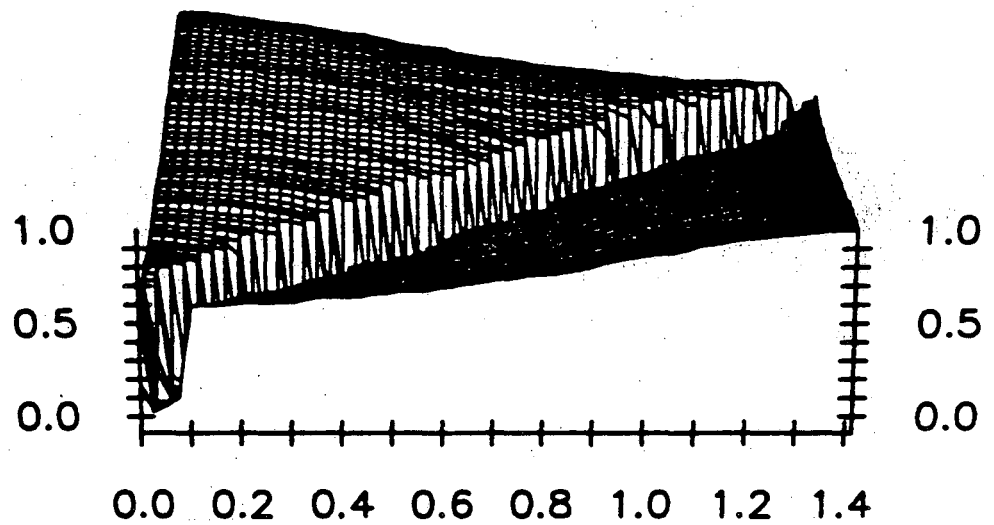

Fig. 9(d)

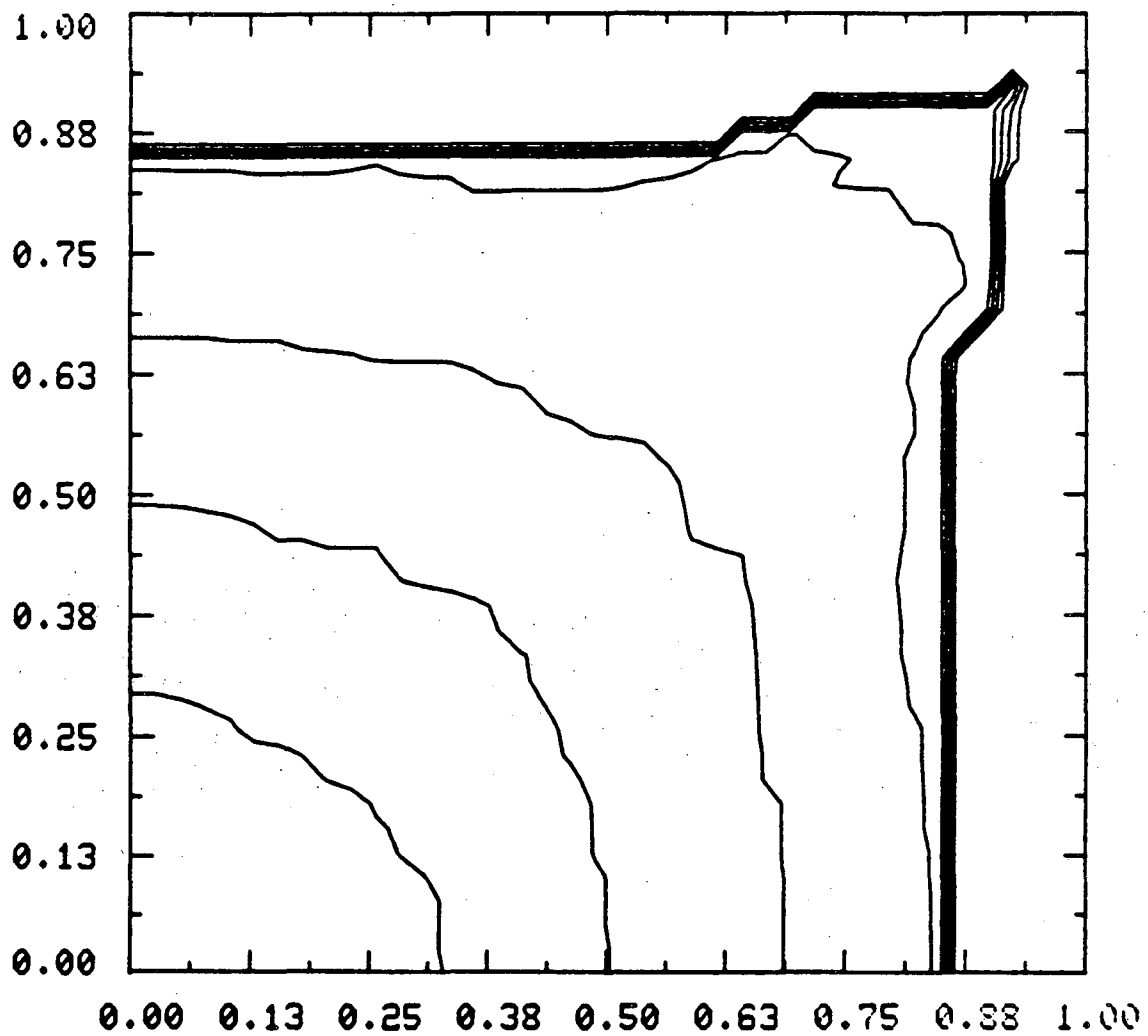
1.00
0.88
0.75
0.63
0.50
0.38
0.25
0.13
0.00
0.00 0.13 0.25 0.38 0.50 0.63 0.75 0.88 1.00

Fig. 10(a)

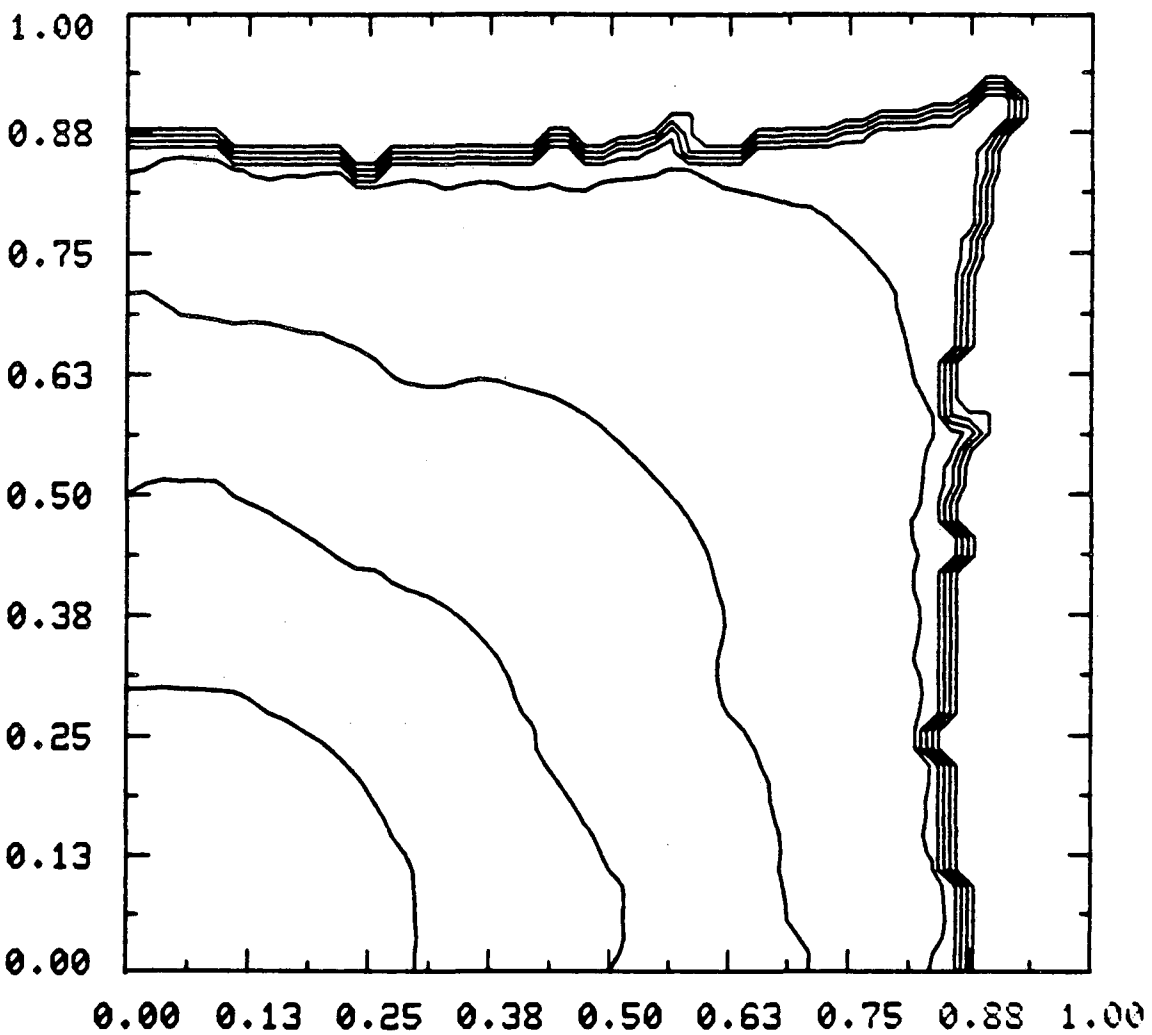
1.00
0.88
0.75
0.63
0.50
0.38
0.25
0.13
0.00
0.00 0.13 0.25 0.38 0.50 0.63 0.75 0.88 1.00

Fig. 10(b)

TECHNICAL INFORMATION DEPARTMENT
LAWRENCE BERKELEY LABORATORY
UNIVERSITY OF CALIFORNIA
BERKELEY, CALIFORNIA 94720